Earthquake Research Advances 5 (2025) 100377

Contents lists available at ScienceDirect

Earthquake Research Advances

journal homepage: www.keaipublishing.com/en/journals/earthquake-research-advances

Rapid disaster assessment of a *M* 6.8 earthquake in Dingri, Xizang, China

Can Zhang [a], Hongme Guo [a,*], Dongming Wang [b], Yuping Yang [a], Zhen Zhao [a], Ying Zhang [a], Zonghang He [a]

[a] Sichuan Earthquake Agency, Chengdu, 610041, China
[b] China Earthquake Disaster Prevention Center, Beijing, 110105, China

ARTICLE INFO

Keywords:
Dingri earthquake
Seismic intensity
Death assessment
Earthquake emergency

ABSTRACT

We conducted a rapid seismic intensity assessment of a *M* 6.8 earthquake in Dingri, Xizang, using a ground motion parameter attenuation model based on the shortest fault distance combined with either an empirical equation for the surface rupture length or data on the aftershocks that occurred within 1.5 hr after the earthquake. The assessment showed that the empirical equation for the relationship between the surface rupture length and magnitude established by Wells et al. yielded a surface rupture length that was closer to the actual value, while the seismic intensity determined using a combination of the ground motion parameter attenuation model and the empirical equation for the surface rupture length was relatively in line with the intensity from the actual investigation. This study also demonstrated that manual intervention and screening are needed for aftershocks within 1.5 hr after the earthquake if this information is to be employed in the intensity assessment. In addition, if the death assessment model does not consider the seismic vulnerability of local buildings, significant errors can occur in practice. Nevertheless, the disaster assessment results were obtained within 5 min after the earthquake, thus providing important data support for the government emergency command and decision-making associated with the emergency rescue response.

1. Introduction

Rapid assessment of seismic intensity following destructive earthquakes is critical for determining impact scope, damage extent, and subsequent emergency resource allocation. While China's National Earthquake Data Center maintains 1 178 operational seismic stations (as of 2023) enabling real-time data collection, most regions still lack dense strong-motion instrumentation for direct intensity measurement. Consequently, the prevailing operational approach relies on elliptical intensity attenuation models derived from statistical regression of historical isoseismal data. However, these conventional models exhibit significant limitations by failing to incorporate region-specific seismic characteristics such as hanging wall effects, rupture directivity, and local soil amplification. This simplification results in regularly elliptical intensity distributions that often diverge substantially from observed patterns, particularly for major earthquakes (M≥7.0). The 2008 M8.0 Wenchuan earthquake serves as a prominent case demonstrating these systematic discrepancies between modeled and actual intensity distributions.

In recent years, the spatial distribution of seismic intensity and identification of the hardest-hit areas have been determined very quickly after a major earthquake by combining the use of empirical equations for the relationship between regional intensity attenuation and the surface rupture length, real-time seismology such as inverse projection, and measurements of aftershocks within 1.5 hr after the earthquake (Zhang et al., 2022; Chen et al., 2022a, 2022b; Zhao et al., 2022, 2023; Wu et al., 2025). Using these estimates, a death assessment model can be employed to predict the number of deaths within the disaster area, providing a reference for the earthquake emergency response, particularly the allocation of emergency rescue teams and supplies during the disaster and directions for improvement to the emergency command and rescue systems run by the government and emergency management departments at all levels.

In the present study, the seismic intensity of a 6.8-magnitude earthquake in Dingri, Xizang, China was rapidly assessed using a ground motion parameter attenuation model based on the shortest fault distance combined with either an empirical equation for the surface rupture length or aftershock measurements taken within 1.5 hr after the

* Corresponding author.
E-mail address: 115453242@qq.com (H. Guo).
Peer review under the responsibility of Editorial Board of Earthquake Research Advances.

https://doi.org/10.1016/j.eqrea.2025.100377
Received 20 February 2025; Received in revised form 31 March 2025; Accepted 31 March 2025
2772-4670/© 2025 China Medical Cosmetology Press Co. Ltd. Publishing services by Elsevier B.V. on behalf of KeAi Communications Co. Ltd. This is an open access article under the CC BY-NC-ND license (http://creativecommons.org/licenses/by-nc-nd/4.0/).

earthquake. A death assessment model for the southwest region of China was then employed to predict the number of deaths based on the results of this attenuation model. This study demonstrates that accurate assessment results can be obtained within 5 min after an earthquake, providing important information for emergency response.

2. Overview of the disaster area

According to the China Earthquake Network Center, at 9:05 a.m. Beijing time on January 7, 2025, an earthquake occurred in Tsogo Township, Dingri County, Shigatse City, Xizang Autonomous Region (28.50°N, 87.45°E), with a magnitude of 6.8 on the Richter scale (moment magnitude: M_W 7.1) and a focal depth of 10 km. Fig. 1 presents the location of the disaster area. The epicenter was located in Dingri County, to the south of Shigatse City (84°20'E–87°70'E, 27°80'N–29°10'N). This region is a plateau area comprising 11 townships and 2 towns under its jurisdiction, with a permanent population of 61 800, a total area of approximately 13 860 km^2, and a population density of around 4.5 persons/km^2. The terrain in the disaster area is high and steep, with an average altitude of about 5 000 m.

This area is located within the Himalayan block of the Gondwana–Himalayan orogenic system and belongs to the secondary tectonic unit of the North Himalayan carbonate platform. Under the influence of the collision between the Indian and Eurasian Plates, a stress field with coexisting north–south compression and east–west tension has been created, generating a significant tectonic activity zone in the southern part of the Qinghai–Xizang Plateau (Bai et al., 2025). There are multiple active faults within the area, including the Chazangcuo fault, the Qingdu fault, the southern section of the Dingjie fault, the Guojia fault, and the Dengmocuo fault, leading to strong seismic activity (Huang et al., 2024). The fault responsible for the case study earthquake was the Dengmocuo fault, which is a normal fault that is the main seismogenic fault around Dingri County and runs in an approximate north–south direction (Li et al., 2024; Tan et al., 2025).

3. Research methods

3.1. Ground motion parameter attenuation model based on the shortest fault distance

A ground motion parameter attenuation model based on the shortest fault distance was established based on a seismic dynamic database containing hundreds of strong earthquake records. This model considers the influence of earthquake magnitude, fault type, hanging wall effects, and site effects on ground motion attenuation characteristics, and thus it can predict ground motion distribution more accurately (Hongjun and Saburoh, 1999). This model has been previously verified using the Wenchuan and Yushu earthquakes and has also been successfully applied to numerous destructive earthquakes, including the Maduo and Jishishan earthquakes (Zhang et al., 2021; Chen et al., 2022a,b; Jia et al., 2024). In the present study, this model was used to generate more than 210 000 calculated kilometer grids centered on the epicenter, corresponding to a calculation area of 210 000 km^2. The ground motion parameters for each of these kilometer grids were then calculated by identifying the nearest rupture fault or seismic energy release point for each grid (i.e., the fault equidistant interval points or aftershock points within 1.5 hr after the

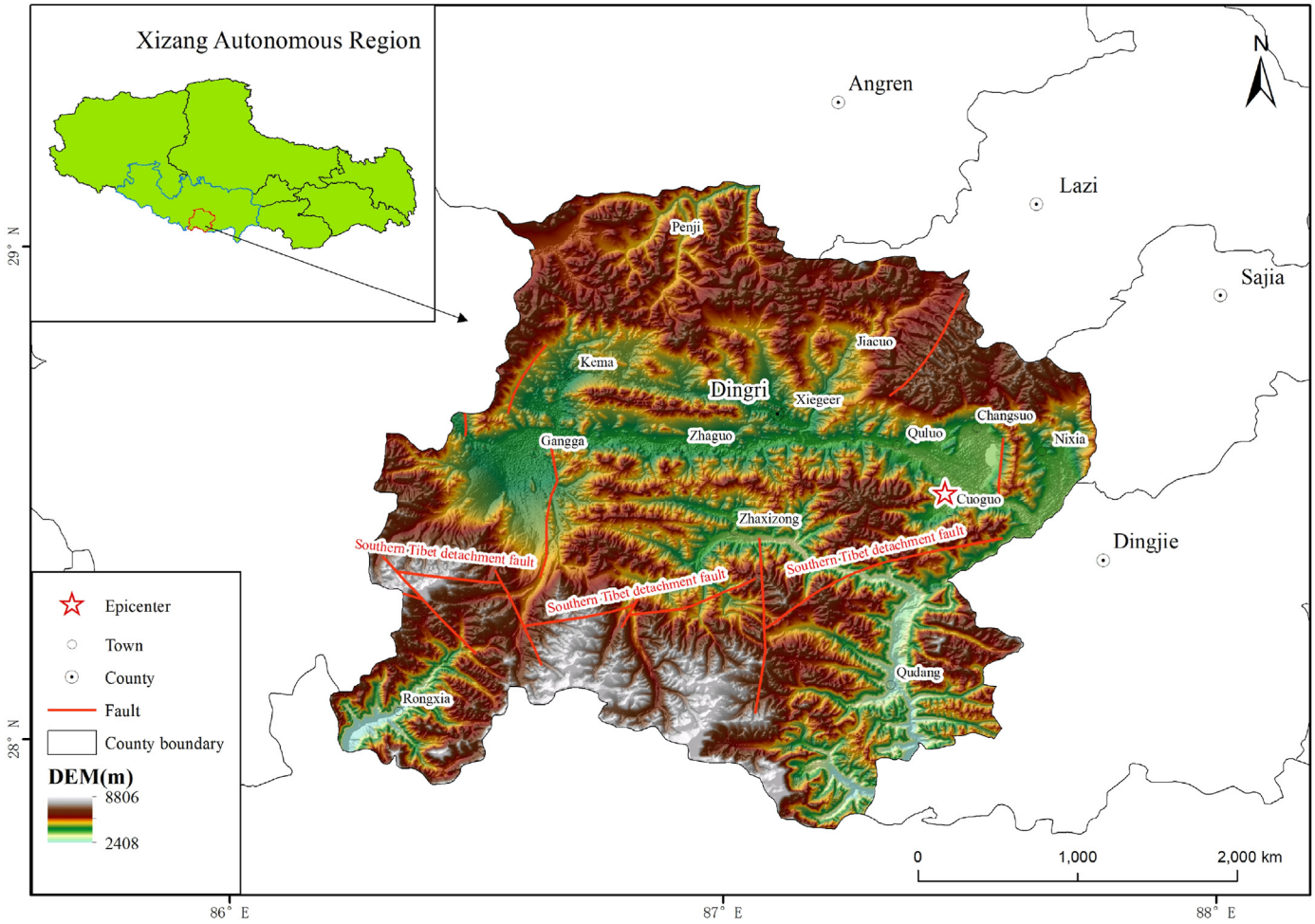

Fig. 1. Location of the disaster area.

earthquake) as follows:

$$\log_{10}\mathrm{PGA} = 0.50Mw + 0.0043D - \log_{10}\left(\mathrm{R} + 0.0055 \cdot 10^{0.5Mw}\right) - 0.003R + 0.61 \quad (1)$$

$$\log_{10}\mathrm{PGV} = 0.58M_{\mathrm{W}} + 0.0038D - \log_{10}\left(R + 0.0028 \cdot 10^{0.5M_{\mathrm{W}}}\right) - 0.002R - 1.29 \quad (2)$$

$$\log_{10}\ \mathrm{AMP} = 1.83 - 0.66\log_{10}\ V_{S30} \quad (3)$$

$$\mathrm{PGV}_{V_{S30}} = \mathrm{AMP} \cdot \mathrm{PGV} \quad (4)$$

In Eqs. (1)–(4), PGA is the peak acceleration of the earthquake (m/s^2), PGV is the peak velocity of the earthquake (m/s), PGV$_{VS30}$ is the peak velocity taking into account site effects (m/s), M_{W} is the moment magnitude of the earthquake, D is the focal depth (km), R is the shortest distance to the rupture fault (km), AMP is the amplification coefficient taking into account site effects, and V_{sS30} is the equivalent shear wave velocity within a depth range of 30 m below the surface. The calculations were based on the value for each kilometer grid.

3.2. Empirical relationship between the surface rupture length and earthquake magnitude

Post-earthquake estimates of the surface rupture length need to be accurate to ensure that the results from the ground motion attenuation model are reliable. Wells et al. (Wells and Coppersmith, 1994) summarized the empirical relationships between earthquake rupture parameters and the magnitude for different types of faults based on the focal parameters of historical earthquakes from around the world. These relationships have been used in a variety of applications. Given that the Dingri earthquake originated from a normal fault, the present study employed the empirical equation for normal faults (Eq. (5)), which is applicable to earthquakes with magnitudes of M 5.2–7.3:

$$M = 4.86 + 1.32\log_{10} L \quad (5)$$

Where M is the Richter magnitude of the earthquake, and L is the surface rupture length (km).

3.3. Death assessment models

3.3.1. Li Wen model

Based on regional differences in earthquake disasters, population distribution differences, and the seismic resistance levels of different regions in China, Li Wen (Li, 2019) divided the population density levels in the northwest, southwest, and east regions, introduced disaster area and seismic fortification intensity levels of VI and above, and established an intensity-based death assessment model specific for different regions or population densities as presented in Eq. (6):

$$\mathrm{D} = e^{b_0 + b_1 I + b_2 S + b_3 \Delta I} \quad (6)$$

where D is the number of deaths caused by the earthquake, I is the epicenter intensity, S is the area of the earthquake zone (km^2), ΔI is the difference between the epicenter intensity and the local seismic fortification intensity, and b_0, b_1, b_2, and b_3 are regression coefficients. The model values for the southwest region are presented in Table 1.

Table 1
Parameters for the Li Wen death assessment model for the southwest region.

Population density (persons/km^2)	b_0	b_1	b_2	b_3	R^2
$\rho \le 60$	−23.390	3.230	−0.000030	−0.980	0.965
$60 \le \rho \le 150$	4.926	−0.762	0.000300	1.559	0.980
$\rho > 150$	−10.485	1.763	0.000006	−0.276	0.980

3.3.2. Emergency assessment of earthquake disasters (GB/T 30352-2013)

Given the impact of the earthquake intensity on casualties and the uneven distribution of people within intensity zones, the Emergency Assessment of Earthquake Disasters (GB/T 30352-2013) established a seismic death assessment model for different intensity zones (Institute of Engineering Mechanics, China Earthquake Administration, Tianjin Earthquake Agency, Xinjiang Uygur Autonomous Region Earthquake Agency, 2013). This model counts the number of deaths in different intensity zones using Eq. (7):

$$N_D = \sum_{j=6}^{I_{max}} A_j R_j \quad (7)$$

where N_D is the number of deaths, $I_{\max}$ is the epicenter intensity, A_j is the area of the j-level intensity zone (km^2), and R_j is the mortality rate corresponding to the j-level intensity zone, as calculated using Eq. (8):

$$\ln R_j = -44.466 + 14.33\ ln\ I_j + 0.960\ ln\ \rho \quad (8)$$

where I_j is the intensity for the j-level intensity zone, and ρ is the population density (persons/km^2).

4. Results and analysis

In the present study, the ground motion parameters for a 6.8-magnitude earthquake in Dingri were determined using a ground motion parameter attenuation model based on the shortest fault distance combined with either the surface rupture length or aftershocks measured within 1.5 hr after the earthquake. As shown in Table 2 and Fig. 2, the study classified the seismic intensity according to the corresponding range of values for the ground motion parameters using the Chinese seismic intensity scale and compared these results with the seismic intensity diagrams obtained from on-site investigations. Based on the calculated seismic intensity distribution, a death assessment was conducted using two death assessment models.

4.1. Rapid assessment of seismic intensity based on the fault rupture scale

Using Eq. (5), the surface rupture length of the M 6.8 earthquake in Dingri was estimated to be 29 km, which was very close to the 26 km surface rupture length determined by the actual investigation. The seismic intensity based on PGA, PGV, and PGV$_{VS30}$ classification (hereinafter referred to as surface rupture PGA, surface rupture PGV, and surface rupture PGV$_{VS30}$, respectively) was calculated using the ground motion parameter attenuation model based on the shortest fault distance in combination with the predicted surface rupture point. As illustrated in Fig. 3, all three seismic intensities ran in a north–northeast direction and were consistent with the actual recorded intensity.

Areas with a seismic intensity of VIII and above are generally considered to be the hardest-hit areas. These hardest-hit areas tend to be

Table 2
Seismic intensity comparison (Chinese seismic intensity scale GB/T 17742-2020) (Institute of Engineering Mechanics of China Earthquake Administration, Earthquake Administration of Fujian Province, Institute of Geophysics of China Earthquake Administration, 2020).

Seismic intensity	Seismic peak acceleration (PGA) (m/s^2)	Seismic peak velocity (PGV) (m/s)
V	0.319(0.223–0.456)	0.0259(0.0177–0.0380)
VI	0.653(0.457–0.936)	0.0557(0.0381–0.0817)
VII	1.350(0.937–1.940)	0.1200(0.0818–0.1760)
VIII	2.790(1.950–4.010)	0.2580(0.1770–0.3780)
IX	5.770(4.020–8.300)	0.5550(0.3790–0.8140)
X	11.900(8.310–17.200)	1.1900(0.8150–1.7500)

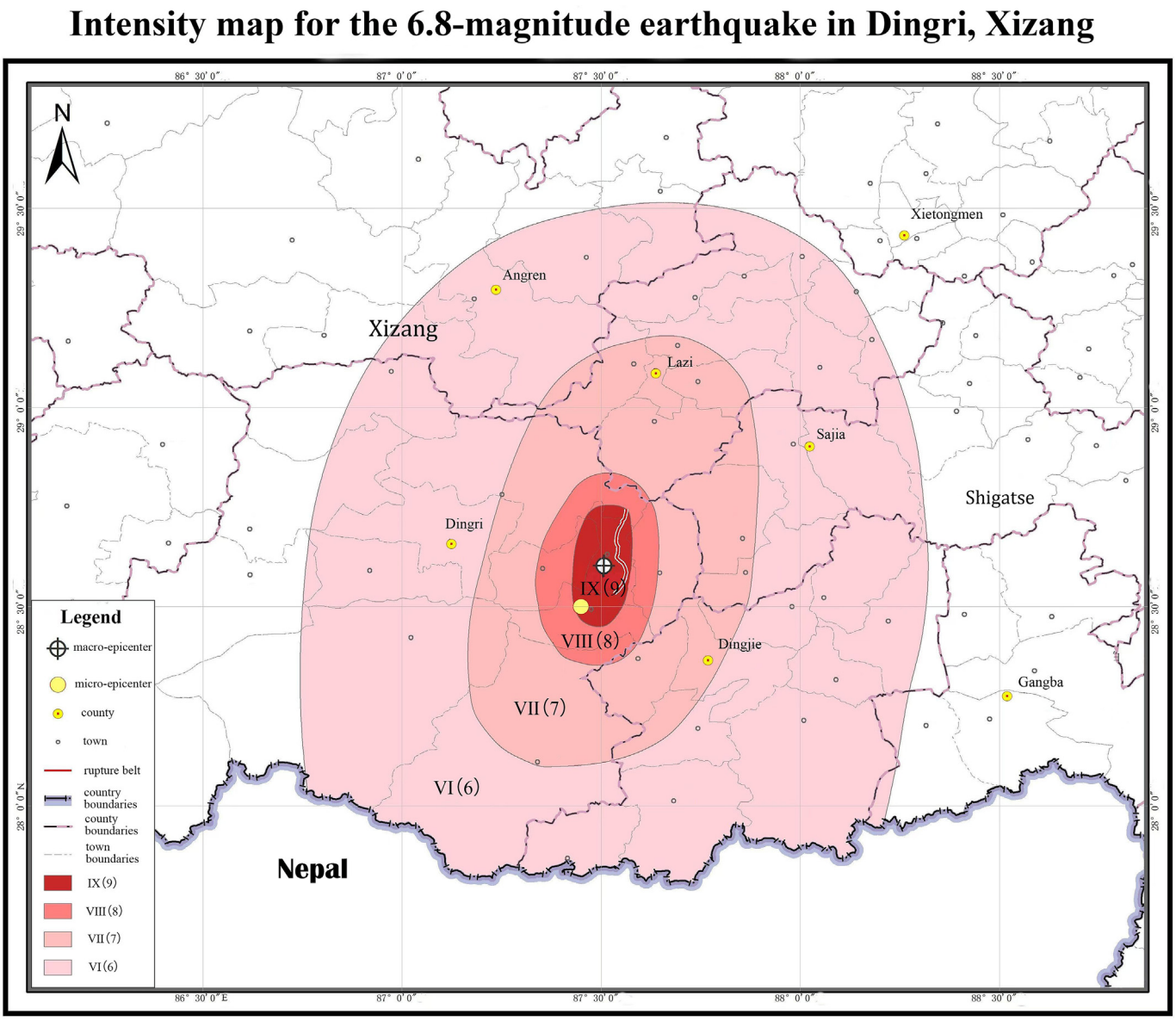

Fig. 2. Intensity map for the *M* 6.8 earthquake in Dingri, Xizang. (Ministry of Emergency Management of the People's Republic of China. https://www.mem.gov.cn/xw/yjglbgzdt/202501/t20250110_517756.shtml).

the focus of post-earthquake emergency rescue, and thus it is important to identify these areas accurately. In the present study, the highest seismic intensity determined based on the calculated surface rupture PGA and surface rupture PGV values was IX, which was the same as the highest recorded intensity. The estimated values for the surface rupture PGA were generally higher than those for the surface rupture PGV. The assessment in the extremely seismic zone yielded relatively accurate results for both the surface rupture PGA and surface rupture PGV. Specifically, the areas estimated to have an intensity level of VIII in the assessment generally overlapped with the areas classified as VIII in the real investigation. In comparison, there was a deviation between the estimated intensities for the IX areas and the corresponding intensities from the actual investigation, which was ascribed to differences between the distribution of faults and the actual rupture location.

The highest seismic intensity determined using site-corrected surface rupture PGV_{VS30} was X, which was one level higher than the intensity from the actual investigation, but the area with the highest intensity was lower than the corresponding area in the actual situation. In contrast, the assessed intensities for areas with intensities above VI were consistent with the corresponding intensities from the actual investigation, and the estimated hardest-hit areas also covered areas near the macro-epicenter. Overall, the assessment accuracy was improved to a certain extent using the proposed model, and towns and villages that were most strongly affected by the earthquake were able to be quickly identified after it struck.

4.2. *Rapid assessment of the seismic intensity based on aftershocks*

Aftershocks within 1.5 hr after the earthquake can be used to characterize the release process of seismic energy roughly. By 10:00 a.m. on January 10, 2025, the *M* 6.8 earthquake in Dingri, Xizang, has caused more than 1600 aftershocks, including 38 aftershocks of *M* 3.0 or above. Within 1.5 hr after the earthquake, there were 14 aftershocks of *M* 2.0 or above, including 7 of *M* 3.0 or above, 5 of *M* 4.0 or above, and 1 of *M* 5.0 or above (Table 3).

The seismic intensity based on PGA, PGV, and PGV_{VS30} classification (hereinafter referred to as aftershock PGA, aftershock PGV, and aftershock PGV_{VS30}, respectively) was calculated using the ground motion parameter attenuation model based on the shortest fault distance in

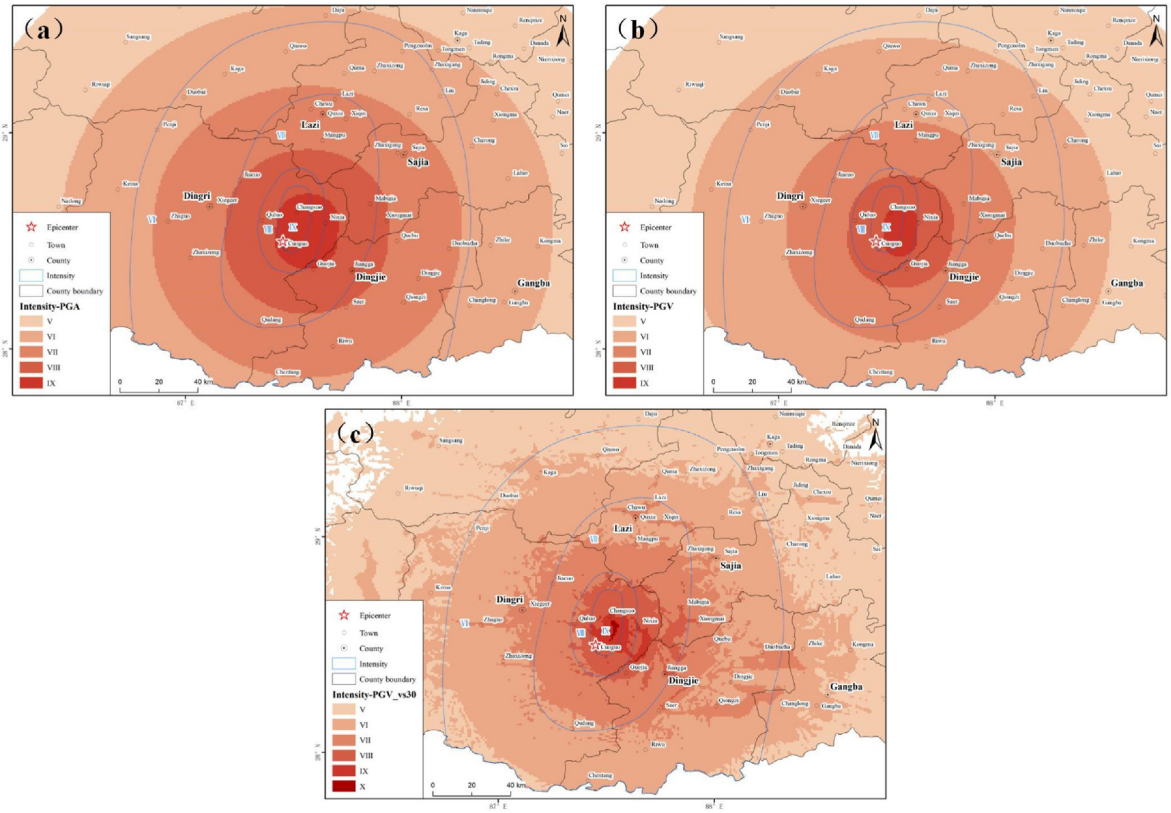

Fig. 3. Results of seismic intensity assessment based on surface rupture points: (a) surface rupture PGA, (b) surface rupture PGV, and (c) surface rupture PGV_{vs30}.

Table 3
Aftershocks recorded within 1.5 hr after the Dingri earthquake.

No.	Time	Latitude and longitude	Magnitude (*M*)	Focal depth (km)
1	January 7, 2025 09:14:41	87.510°N, 28.560°E	5.1	14.7
2	January 7, 2025 09:37:99	87.303°N, 28.682°E	4.3	11.9
3	January 7, 2025 09:31:57	87.460°N, 28.845°E	4.3	2.3
4	January 7, 2025 09:32:01	87.543°N, 28.878°E	4.3	14.3
5	January 7, 2025 09:43:53	87.361°N, 28.593°E	4.2	52.5
6	January 7, 2025 09:24:25	87.508°N, 28.586°E	4.2	1.7
7	January 7, 2025 10:01:06	87.518°N, 29.117°E	3.9	38.7
8	January 7, 2025 09:59:47	87.465°N, 28.908°E	3.9	18.8
9	January 7, 2025 10:32:39	87.464°N, 28.566°E	3.7	41.5
10	January 7, 2025 10:04:06	87.531°N, 28.951°E	3.6	15.8
11	January 7, 2025 10:27:27	87.445°N, 28.764°E	3.5	15.2
12	January 7, 2025 10:22:42	87.442°N, 28.723°E	3.4	15.5
13	January 7, 2025 10:02:12	87.414°N, 28.750°E	3.4	14.4
14	January 7, 2025 10:20:35	87.457°N, 28.961°E	2.9	15.7

combination with aftershocks within 1.5 hr after the earthquake. Consistent with the actual intensity, each of the three seismic intensities runs in a north–northeast direction (Fig. 4).

In Fig. 4, the green dots represent the aftershock points within 1.5 hr after the earthquake. As shown in Fig. 4(a)–(c), the distribution of aftershocks was consistent with the direction of the seismic energy release and rupture. The highest seismic intensity level was estimated to be IX based on the aftershock PGA and aftershock PGV. This was relatively high due to the scattered distribution of aftershocks, but the extent of the extreme seismic zone was still accurately delineated. The assessment using the site-corrected aftershock PGV_{VS30} also identified a small area with an intensity level of X to the northeast of the epicenter. The predicted extent of the extreme seismic zone in this assessment aligned well with the actual investigation results, albeit with minor discrepancies. Therefore, manual review and filtering were still necessary to exclude aftershock points showing significant deviation, so as to improve the accuracy of intensity predictions based on aftershock data.

4.3. Rapid disaster assessment and comparative analysis

We compared the seismic intensities experienced by towns in the hardest-hit areas based on the on-site investigation with those estimated using the surface rupture and aftershock PGV_{VS30} values from our rapid assessment approach (Table 4).

All of the townships except Jiacuo included in the IX intensity zone based on the surface rupture PGV_{vs30} assessment were consistent with townships from the on-site investigation. The extent of Jiacuo classified within the IX level intensity zone by the actual investigation was almost negligible. Likewise, the townships included in the VIII intensity zone based on the surface rupture PGV_{vs30} assessment were consistent with those from the actual investigation. Similarly, the townships included in the extreme seismic zone determined using the aftershock PGV_{vs30} assessment were the same as those identified by the actual investigation. Notably, the size of each intensity zone was relatively large and included many towns. Overall, the calculation based on surface rupture PGV_{vs30} or

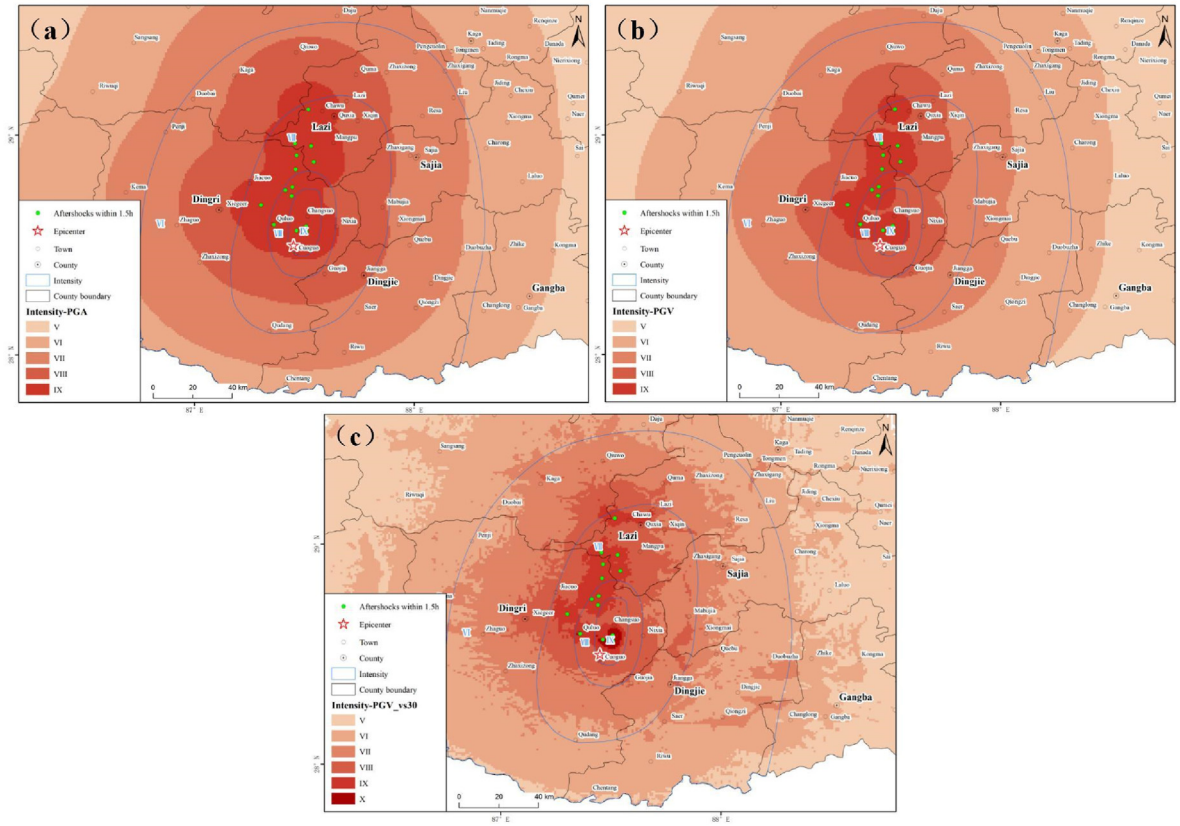

Fig. 4. Results of seismic intensity assessment based on aftershocks within 1.5 hr after the earthquake: (a) aftershock PGA, (b) aftershock PGV, and (c) aftershock PGV_{vs30}.

Table 4
Comparison of the predicted townships and towns from the actual investigation in the hardest-hit areas.

Seismic intensity level	On-site investigation	Surface rupture PGV_{VS30}	Aftershock PGV_{VS30}
X	None	Changsuo township, Cuoguo township	Changsuo township, Quluo township, Cuoguo township
IX	Changsuo township, Quluo township, Cuoguo township, Nixia township, Jiacuo township	Changsuo township, Quluo township, Cuoguo township, Nixia township	Changsuo township, Quluo township, Cuoguo township, Chawu township, Mangpu township
VIII	Changsuo township, Quluo township, Cuoguo township, Nixia township, Jiacuo township, Qudang township, Guojia township, Mangpu township	Changsuo township, Quluo township, Cuoguo township, Nixia township, Jiacuo township, Qudang township, Guojia township, Mangpu township, Mabujia township, Xiongmai township, Quebu township, Jiangga town	Changsuo township, Quluo township, Cuoguo township, Nixia township, Jiacuo township, Qudang township, Guojia township, Mangpu township, Mabujia township, Xiongmai township, Quebu township, Jiangga town, Xiegeer town, Kaga town, Quma township, Lazi town

aftershock PGV_{vs30} produced accurate results when assessing the size of the extreme seismic zone, especially for the three key townships Changsuo, Quluo, and Cuoguo. Therefore, if the proposed assessment was employed, townships within the high-intensity zone would not fail to receive timely government assistance during the post-earthquake emergency response.

In terms of the area and overlap for each seismic intensity zone, the calculation based on surface rupture PGV_{VS30} produced area sizes that were more consistent with the actual situation (Table 5). This approach also achieved an overlap of 97.7 % in the VIII intensity zone between the model estimates and reality, representing a more accurate prediction of the extent of the hardest-hit areas. In comparison, the area estimates based on aftershock PGV_{VS30} were larger for each intensity zone compared to the actual situation, with an overlap of only 77.1 % for intensity zones with a level of IX and above. Therefore, although aftershock PGV_{VS30}-based assessment outperformed surface rupture PGV_{VS30}-based assessment, the former had a lower accuracy when estimating the VII intensity zone. Given that the fault structure and focal mechanism of this earthquake were relatively simple, the rapid assessment of seismic intensity based on the fault rupture scale under the premise of accurately predicting the length of the surface rupture can be used to more accurately assess the seismic intensity than the assessment based on aftershock data within 1.5 hr after the earthquake.

We also conducted a death assessment using two death assessment models based on the surface rupture PGV_{VS30} and aftershock PGV_{VS30} estimates (Table 6).

After an earthquake, determining the number of casualties is an

Table 5
Comparison of the area size and overlap of seismic intensity zones above intensity level VII (km^2).

Seismic intensity level	On-site investigation	Surface rupture PGV_{VS30}		Aftershock PGV_{VS30}	
	Area	Area	Overlap	Area	Overlap
≥IX	411	463	62.3 %	1547	77.1 %
VIII	869	2069	97.7 %	4962	93.2 %
VII	5350	8371	88.6 %	12,226	60.1 %

important basis for classify the earthquake disaster response levels and for the allocation of resources and rescue forces. Under the Li Wen model, the seismic intensity assessment based on surface rupture PGV_{VS30} and aftershock PGV_{VS30} predicted 40 and 91 deaths, respectively. The reason for the large difference in the number of deaths between the two assessments is that the Li Wen model is established mainly based on the size of the disaster area, with an intensity level of VI or above and seismic fortification intensity. This difference can also be attributed to the large difference in the area range for each seismic intensity zone between the two assessments.

Under the earthquake disaster emergency assessment model, the seismic intensity assessment based on surface rupture PGV_{VS30} and aftershock PGV_{VS30} predicted 53 and 72 deaths, respectively, which were not significantly different from those predicted by the Li Wen model. The predicted numbers of deaths based on these two death assessment models were all below the actual death toll of 126, though they were within the same order of magnitude. These results are mainly attributable to the considerable difference between the seismic fortification intensity of local buildings and the corresponding standards. The seismic fortification intensity of buildings in Shigatse City is set at grade 8. However, most of the residential buildings in the epicenter area were earth–wood structures or brick (stone)–wood structures, which do not meet the local seismic fortification standards (Wang et al., 2025), and a large proportion of the buildings collapsed in the earthquake due to their relatively weak seismic resistance (Tan et al., 2025). Additionally, both assessment models failed to take into account influencing factors such as the seismic vulnerability matrix of local buildings, resulting in a significant discrepancy between the predicted number of deaths and the actual death toll.

5. Conclusion and discussion

In this study, we conducted a rapid assessment of the seismic intensity of the 6.8-magnitude earthquake in Dingri, Xizang using a ground motion parameter attenuation model based on the shortest fault distance, an empirical equation for the surface rupture length, and aftershocks within 1.5 hr after the earthquake. Furthermore, we estimated the number of deaths based on the results of the intensity assessment. A comparative analysis of the predicted seismic intensity and number of deaths, along with the corresponding actual data, provided us with several important insights.

First, for earthquakes with relatively simple seismogenic structures, the combined use of the ground motion parameter attenuation model and the surface rupture length relationship equation can yield accurate assessment results for the seismic intensity and death toll within 5 min after the official report of the earthquake's occurrence. This approach can thus provide reference data for emergency command and rescue decisions in the shortest time. In comparison, the combination of the ground motion parameter attenuation model and aftershocks within 1.5 hr after the earthquake was shown to be more suitable for assessing earthquakes with complex seismogenic structures and unclear rupture directions.

Second, the surface rupture length predicted using the empirical equation for the relationship between the surface rupture length and magnitude was very close to the actual value. The predicted seismic intensity based on the empirical equation in combination with the ground motion parameter attenuation model was more consistent with the intensity determined during the actual investigation. In contrast, the seismic intensity determined by the combined use of aftershocks 1.5 hr after the earthquake and the ground motion parameter attenuation model differed from the actual intensity because the aftershocks were relatively scattered. In this case, manual intervention and screening were needed to improve the accuracy of the assessment. For this purpose, the PGV integrating site effects can more realistically reflect the spatial distribution characteristics of seismic intensity. In addition, the death assessment model that failed to consider the seismic vulnerability of local buildings produced a large error compared to the actual death toll.

Table 6
Comparison between the results of the death assessment and real data.

Assessment model	Actual number of deaths	Surface rupture PGV_{vs30}	Aftershock PGV_{vs30}
Li Wen model	126	40	91
Emergency assessment of earthquake disasters	126	53	72

Despite the important findings of the present study, a number of issues still need to be addressed. Given that the seismic intensity attenuation model for ground motion parameters is relatively dependent on the seismogenic fault, the nature and direction of the seismogenic fault should be carefully established in practical applications. The accuracy of the seismic intensity assessment can also be improved by comprehensively analyzing the attenuation model, real-time seismology such as inverse projection, and the distribution characteristics of aftershocks.

In addition, the intensity values predicted by the ground motion parameter attenuation model based on the shortest fault distance were generally larger than the actual intensity values. This deviation may be due to the fact that the ground motion parameter attenuation model was established based on research data from Japan. Thus, although this ground motion parameter attenuation model has achieved good results when applied to other destructive earthquakes, the parameters of the model still need to be optimized for southwest China.

In the present study, the V_S30 data used to calculate the PGV with site effects originated from the USGS, which may introduce some inaccuracies when used in China. The accuracy of this model in the rapid assessment of seismic intensity can thus be improved by developing vs30 data that is more applicable to the Chinese region (Zhang et al., 2024). In addition, more influencing factors, such as the vulnerability of local buildings, should be taken into account for death assessment.

CRediT authorship contribution statement

Can Zhang: Formal analysis. **Hongme Guo:** Project administration. **Dongming Wang:** Investigation. **Yuping Yang:** Data curation. **Zhen Zhao:** Data curation. **Ying Zhang:** Investigation. **Zonghang He:** Conceptualization.

Declaration of competing interest

The authors declare that they have no known competing financial interests or personal relationships that could have appeared to influence the work reported in this paper.

Author agreement and Acknowledgement

All authors agree for this publication. We would like to thank the China Earthquake Disaster Prevention Center, Seismic Active Fault Survey Data Center (https://www.activefault-datacenter.cn), Dingri Earthquake Scientific Expedition Team of China University of Geosciences, China Earthquake Networks Center and USGS (https://www.usgs.gov) for providing data support.

This study was supported by the National Key R&D Program of China (2020YFA07106003), the National Natural Science Foundation of China (42061073), and the Innovation Team of Sichuan Earthquake Agency (202401).

References

Bai, L., Chen, Z., Wang, S., 2025. The 2025 Dingri MS6.8 earthquake in Xizang: analysis of tectonic background and discussion of source characteristics. Reviews Geophys. Planet Phys. 56 (3), 258–263.

Chen, W., Wang, D., Si, H., et al., 2022a. Rapid estimation of seismic intensities using a new algorithm that incorporates array technologies and ground-motion prediction equations (GMPEs). Bull. Seismol. Soc. Am. 112 (3).
Chen, W., Wang, D., Zhang, C., et al., 2022b. Estimating seismic intensity maps of the 2021 Mw 7.3 Madoi, Qinghai and Mw 6.1 Yangbi, Yunnan, China earthquakes. J. Earth Sci. 33 (4), 839–846.
Hongjun, S.I., Midorikawa, S., 1999. New attenuation relationships for peak ground acceleration and velocity considering effects of fault type and site condition. J. Archit. Plann. Environ. Eng. 523, 63–70.
Huang, T., Wu, Z., Han, S., et al., 2024. Basic characteristics of active faults and potential risk assessment of earthquake disasters in Shigatse, Tibet. Progr. Earthq. Sci. 54 (10), 696–711.
Institute of Engineering Mechanics of China Earthquake Administration, Earthquake Administration of Fujian Province, Institute of Geophysics of China Earthquake Administration, 2020. GB/T 17742-2020 China Seismic Intensity Scales.
Institute of Engineering Mechanics of China Earthquake Administration, Tianjin Earthquake Bureau, Xinjiang Uygur Autonomous Region Earthquake Bureau, 2013. GB/T 30352-2013 Earthquake Disaster Emergency Assessments.
Jia, Y., Chen, W., Kang, D., et al., 2024. Rapid determination of source parameters of the *M* 6.2 Jishishan earthquake in Gansu Province and its application in emergency response. Earthq. Res. Adv. 4 (4), 11–20.
Li, N., Liu, L., Zhu, L., et al., 2024. Deformation structure of Quaternary soft sediments in the Dingmucuo graben on the northern edge of the Himalayas. J. Chengdu Univ. Technol. (Sci. Technol. Ed.) 51 (6), 1048–1056.
Li, W., 2019. Research on the Vulnerability of Life in Earthquake Disasters. Lanzhou Institute of Seismology, China Earthquake Administration. Doctoral dissertation.
Ministry of Emergency Management of the People's Republic of China. Ministry of Emergency Management of the People'S Republic of China, China Earthquake Administration Release the intensity map of Xizang Dingri 6.8 earthquake[EB/OL]. https://www.mem.gov.cn/xw/yjglbgzdt/202501/t20250110_517756.shtml.
Tan, S., Yang, Y., Xu, Q., et al., 2025. Analysis of Surface Coseismic Deformation Characteristics and Building Damage of the MS 6.8 Strong Earthquake in Dingri County, Tibet on January 7, 2025. Journal of Chengdu University of Technology (Natural Science Edition), pp. 1–11.
Wang, Y., Li, X., Wang, N., et al., 2025. Analysis of the causes of damage to residential buildings in the 6.8-magnitude Dingri earthquake in Tibet. J. Earthq. Eng. 1–12.
Wells, D., Coppersmith, K., 1994. New empirical relationships among magnitude, rupture length, rupture width, rupture area, and surface displacement. Bull. Seismol. Soc. Am. 84 (4), 974–1002.
Wu, J., Chen, W., Jia, Y., et al., 2025. Rapid assessment of seismic intensity and disaster based on dense array - a case study of the Ms6.8 earthquake in Shigatse, Tibet in 2025. Earth Sci. 50 (5), 1770–1781.
Zhang, C., Chen, W., Lin, X., 2022. Earthquake damage simulation of urban buildings based on ground motion parameters–A case study of Chengguan District, Lanzhou City. J. Earthq. Eng. 44 (1), 172–182.
Zhang, C., Chen, W., Si, H., et al., 2021. Rapid intensity assessment of the 7.4 magnitude earthquake in Maduo, Qinghai. J. Earthq. Eng. 43 (4), 876–882.
Zhang, C., Guo, H., Zhao, Z., et al., 2024. Construction and application of vS30 data in Sichuan Province: a case study of the 8.0 magnitude Wenchuan earthquake in Sichuan. J. Earthq. Eng. 1–9.
Zhao, H., Chen, W., Zhang, C., et al., 2023. Rapid estimation of seismic intensities by analyzing early aftershock sequences using the robust locally weighted regression program (LOWESS). Nat. Hazards Earth Syst. Sci. 23 (9), 3031–3050.
Zhao, H., He, S., Chen, W., et al., 2022. Study on rapid assessment method of seismic intensity based on aftershock sequences - a case study of the 6.9 magnitude earthquake in Menyuan, Qinghai. J. Earthq. Eng. 44 (2), 432–439.